Large extrinsic spin Hall effect in Au-Cu alloys by extensive atomic disorder scattering

L. K. Zou,[1] S. H. Wang,[1] Y. Zhang,[1] J. R. Sun,[1] J. W. Cai,[1,*] and S. S. Kang[2]

[1]*Beijing National Laboratory for Condensed Matter Physics and Institute of Physics, Chinese Academy of Sciences, Beijing 100190, People's Republic of China*

[2]*School of Physics, Shandong University, Jinan 250100, People's Republic of China*

(Received 17 November 2015; revised manuscript received 30 December 2015; published 14 January 2016)

Spin Hall angle, which denotes the conversion efficiency between spin and charge current, is a key parameter in the pure spin current phenomenon. The search for materials with large spin Hall angle is indeed important for scientific interest and potential application in spintronics. Here the large enhanced spin Hall effect (SHE) of Au-Cu alloy is reported by investigating the spin Seebeck effect, spin Hall anomalous Hall effect, and spin Hall magnetoresistance of the $Y_3Fe_5O_{12}$ (YIG)/Au_xCu_{1-x} hybrid structure over the full composition. At the near equiatomic Au-Cu composition with maximum atomic disorder scattering, the spin Hall angle of the Au-Cu alloy increases by two to three times together with a moderate spin diffusion length in comparison with Au. The longitudinal spin Seebeck voltage and the spin Hall magnetoresistance ratio also increase by two to three times. More importantly, no evidence of anomalous Hall effect is observed in all YIG/Au-Cu samples, in contrast to the cases of other giant SHE materials Pt(Pd), Ta, and W. This behavior makes Au-Cu free from any suspicion of the magnetic proximity effect involved in the hybrid structure, and thus the Au-Cu alloy can be an ideal material for pure spin current study.

DOI: 10.1103/PhysRevB.93.014422

I. INTRODUCTION

The issue of pure spin current has attracted intense attention recently. It undertakes maximal spin angular momentum with minimal Joule heat thus meeting the energy-saving requirement of high-performance spintronic devices in the future. Several methods have been reported to generate pure spin current, including nonlocal spin valves [1], spin Hall effect [2,3], spin pumping [4–6], and spin Seebeck effect [7]. Predicted decades ago [8,9], spin Hall effect (SHE), referring to the conversion of charge current into pure spin current in nonmagnetic metals, has recently been revived since its first observation in semiconductors with optical methods [10]. Currently SHE has been regarded as a promising way to produce spin current for spin transfer torque application, whereas the reciprocal process of SHE, namely, inverse spin Hall effect (ISHE) [5], has been utilized as a powerful tool to detect spin current. In fact, spin Seebeck effect (SSE) is a phenomenon in which the thermally induced spin current from a ferromagnet is injected into a nonmagnetic metal and is further transformed into electrically detectable voltage via ISHE. So far, Pt [11], Ta, and W with large intrinsic spin Hall angles among the transition metals show distinct advantages in exploring spin current phenomena. However, there is a debate about whether the magnetic proximity effect (MPE) presents or not in Pt as well as in Pd and even in Ta and W when contacting with an insulating ferromagnet [12–14]. As a unique heavy transition metal with the electronic structure far from the Stoner ferromagnetic instability [15,16], Au is commonly considered to have negligible MPE and presents convincing spin current phenomena in hybrid structures. The drawback of Au, in comparison with Pt, Ta, and W, is its much smaller inverse spin Hall voltage due to the very low resistivity of Au.

Extrinsic scattering is the other mechanism to give rise to SHE in addition to the Berry-phase curvature induced intrinsic SHE. Remarkably, large extrinsic SHE has recently been found at low temperature in the diluted alloys of Cu(Bi) [17], Cu(Ir) [18,19], Cu(Pb) [20], and Au(W) through nonlocal spin valves and spin pumping [21]. Since there is almost negligible solid solubility of Bi, Ir, and Pb in Cu and W in Au, these alloys may encounter problems of uniformity, repeatability, and stability with even serious aging effect in the Cu(Pb) samples. Copper possesses a similar band structure with gold and stubborn resistance to ferromagnetism; moreover, Au-Cu can form a solid solution in the full composition range [22]. This means that beyond the studied diluted alloys, the Au-Cu alloy is worth exploring either from fundamental physics or from spintronic application. In this work, we report large extrinsic spin Hall effect in Au-Cu alloy films. In coincidence with the increase of the atomic disorder scattering, the YIG ($Y_3Fe_5O_{12}$)/Au-Cu bilayer system shows considerably enhanced spin Seebeck effect and spin Hall magnetoresistamce (SMR). The spin diffusion length of $Au_{0.6}Cu_{0.4}$ is determined to be 4.6 nm, and the spin Hall angle is about 0.011. This value, consistent with the theoretical prediction [23], is comparable to the reported value of Pt. More importantly, there is no detectable anomalous Hall signal in all YIG/Au-Cu bilayers, eliminating any possibility of the presence of MPE. Therefore, the near equiatomic Au-Cu alloy provides us a real, ideal SHE material for further investigation and applications in spintronics.

II. EXPERIMENT

Single-crystal $Y_3Fe_5O_{12}$ (YIG) films with a (111) surface were grown on $Gd_3Ga_5O_{12}$ (GGG) substrate by liquid-phase epitaxy. Six sets of thin Au-Cu film samples, including Au, $Au_{0.83}Cu_{0.17}$, $Au_{0.6}Cu_{0.4}$, $Au_{0.48}Cu_{0.52}$, $Au_{0.39}Cu_{0.61}$, and $Au_{0.19}Cu_{0.81}$ with thickness ranging from 2.5 to 60 nm, were deposited on YIG (or GGG) substrates at room temperature using multisource magnetron sputtering. A 5-nm SiO_2 capping

*jwcai@iphy.ac.cn

layer is adopted to protect the metal films against oxidation. The atomic fraction of Au in Au-Cu alloy was determined by inductively coupled plasma–atomic emission spectroscopy (ICP-AES). The base pressure of the sputtering system was lower than 4×10^{-5} Pa and the working argon pressure was 0.5 Pa. A shadow mask was used to pattern the samples into Hall-bar shape for magnetotransport measurements. Each Hall bar includes a 4.8 mm × 0.5 mm center portion with three perpendicularly placed 1.2 mm × 0.3 mm side bars 1.7 mm apart. Ultrasonic wire bonding (20 μm in diameter) was used for electrode connection. In longitudinal spin Seebeck setup, a temperature difference applied along the z axis between the bottom of the GGG substrate and the top of the film was near 13 K. Spin Seebeck effect was measured on our self-made device with a voltage sensitivity up to 0.1 μV. Hall effect and magnetoresistance measurements were performed in a Quantum Design PPMS-14H. The magnetoresistance measurements were performed in a four-point probe geometry using fields of up to 1 T, with accurancy of $\Delta R/R = 2 \times 10^{-6}$. Unless otherwise specified, all measurements in this work were carried out at room temperature.

III. RESULTS AND DISCUSSION

A. Spin Seebeck voltage

We adopt longitudinal spin Seebeck effect (LSSE) configuration to measure the spin Seebeck voltage (i.e., inverse spin Hall voltage) induced in the Au-Cu layers on the 5.5-μm-thick single-crystalline (111) YIG films [24]. To give a profile about inverse spin Hall effect of Au-Cu alloys, series samples with different Au-Cu composition (including pure Au) were deposited on the YIG films cut from the same specimen. Figures 1(a)–1(h) show field dependence of thermal voltage ($V_{\rm th}$) for the 3- and 7-nm-thick Au, $Au_{0.83}Cu_{0.17}$, $Au_{0.6}Cu_{0.4}$, and $Au_{0.39}Cu_{0.61}$ samples. The offset of the measured thermal voltage caused by the conventional Seebeck effect of the whole heating and measurement system has been subtracted. From these figures, all $V_{\rm th}-H$ curves are similar with each other, and $V_{\rm th}$ becomes saturated at $|H| > 30$ Oe, resembling the $M-H$ curves of the YIG films (not shown). It should be emphasized that the Au-Cu films deposited on the bare $Gd_3Ga_5O_{12}$ (GGG) substrates do not exhibit any thermal voltage variation within ±120 Oe. As an example, the $V_{\rm th}-H$ curve of GGG/$Au_{0.6}Cu_{0.4}$ (3 nm) is included in Fig. 1(c). Therefore, the voltage difference between the opposite YIG moment alignments in the YIG/Au-Cu samples should originate from SSE (or ISHE) of the Au-Cu films. As will be proved later, there is no MPE and thus no anomalous Nernst effect entanglement in the YIG/Au-Cu system. In addition, the dependence of thermal voltage as a function of the YIG moment direction was also examined by rotating the sample in a constant in-plane field of 100 Oe. The inset of Fig. 1(i) shows the $V_{\rm th}$-θ curve of the YIG/$Au_{0.6}Cu_{0.4}$ (3 nm). The experimental data can be perfectly fitted by a sine function of θ, as required by ISHE.

From Figs. 1(a)–1(h), one also notes that the Au_xCu_{1-x} ($x = 0.83, 0.6, 0.39$) samples have a much larger SSE voltage or ISHE signal than the Au samples with the same thickness. Among them, the 3-nm $Au_{0.6}Cu_{0.4}$ sample has an SSE more

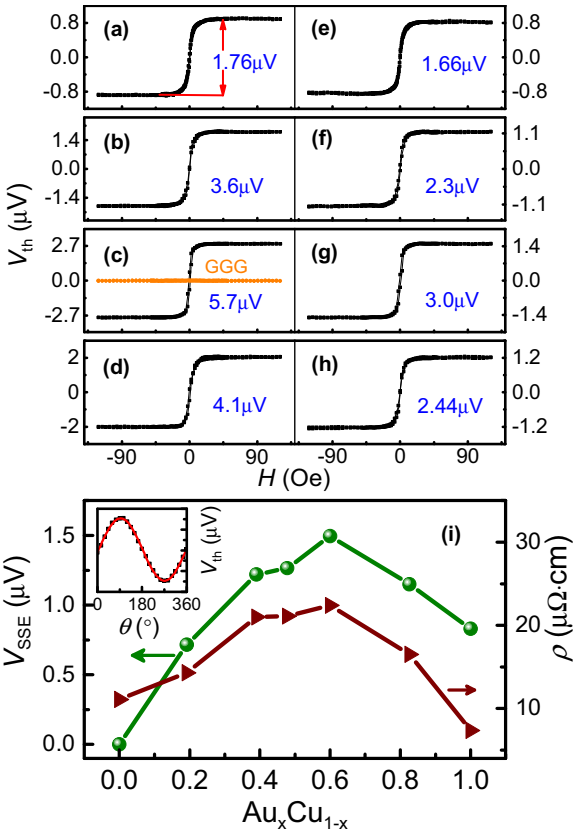

FIG. 1. The H dependence of thermal voltage of Au (a,e); $Au_{0.83}Cu_{0.17}$ (b,f); $Au_{0.6}Cu_{0.4}$ (c,g); and $Au_{0.39}Cu_{0.61}$ (d,h) stemming from spin Seebeck effect in YIG film. The thicknesses of the metal layer are 3 nm (a–d) and 7 nm (e–h), respectively. The orange curve in (c) is the result of GGG/$Au_{0.6}Cu_{0.4}$. (i) Au concentration dependence of spin Seebeck voltage (olive sphere) and resistivity (wine triangle) in YIG/Au-Cu(7 nm). Inset is measured angular dependence of thermal voltage (black square) which can be fitted with a $\sin\theta$ function (red line).

than three times that of the Au sample. Although the SSE enhancement becomes less in the thicker films, the Au_xCu_{1-x} ($x = 0.83, 0.6, 0.39$) samples give a larger signal throughout the studied thickness range from 2.5 to 60 nm with $Au_{0.6}Cu_{0.4}$ always the largest one. When the Au concentration decreases to 19%, the SSE signal is weaker than that for the Au samples, but still observable (not shown). For pure Cu films grown on the YIG films, there is no observable SSE signal, which is in agreement with the results reported previously [11]. It should be pointed out that all Au-Cu alloys present the same SSE voltage polarity and thus have the same SHE sign as Au.

To reveal the SSE enhancement mechanism, the SSE voltage of the 7-nm Au_xCu_{1-x} series samples and their electrical resistivity are compiled in Fig. 1(i). Remarkably, SSE signal and resistivity coincidently increase significantly with the addition of Cu into the Au, and both reach their maximum value at 40% Cu, then they gradually decrease with the further increase of the Cu concentration. This means that the large increase in SSE and resistivity near the equiatomic Au-Cu composition should be triggered by the same cause. As is known, the sputtering deposited Au-Cu film adopts

a chemically disordered face-centered cubic structure [25], and the conduction electrons will experience atomic disorder scattering, so the resistivity of Au increases when alloyed with Cu. Near the equiatomic Au-Cu composition, the resistivity gets a peaked value due to the maximum disorder scattering. Extrinsic scattering is an important source for SHE; it is highly possible that the atomic disorder scattering also gives rise to the SSE or ISHE enhancement. We would like to emphasize that, in disordered ferromagnetic Fe-Pt alloys, anomalous Hall effect (AHE) is also peaked near the equiatomic composition due to the atomic disorder scattering [26]. Considering that SHE shares the same mechanisms with AHE, the observed largest SSE in $Au_{0.6}Cu_{0.4}$ should be ascribed to the intensive atomic disorder scattering.

B. Anomalous Hall effect

Anomalous Hall effect is a hallmark of magnetic conductors. However, for a nonmagnetic metal with large SHE in contact with an insulating ferromagnet, spin Hall AHE with the same behavior of AHE was theoretically derived from the imaginary part of the interface spin mixing conductance [27]; it was thus asserted that the AHE-like signal in the hybrid structure cannot be taken as the criterion for magnetic proximity effect. This has recently led to a serious debate about whether MPE presents or not in YIG/Pt, Ta, and W systems. With only an ordinary Hall signal detected, Au was considered to be free from MPE in the YIG/Au structure [28]. For the present YIG/Au-Cu system, no AHE-like signal is observed for all samples irrespective of the film composition or thickness. Figure 2(a) shows a magnified view of the field dependence of Hall resistance (R_H) at room temperature with the Au_xCu_{1-x} (x = 1, 0.83, 0.6, 0.48, 0.39, 0.19) layers as thin as 2.5 nm. In addition, the high-field Hall resistance loops for a representative Au-Cu sample at 10 K and room temperature are also given in the inset of Fig. 2(a) for completeness. The straight lines of all R_H-H loops strongly suggest that the YIG/Au-Cu system is free from MPE together with null

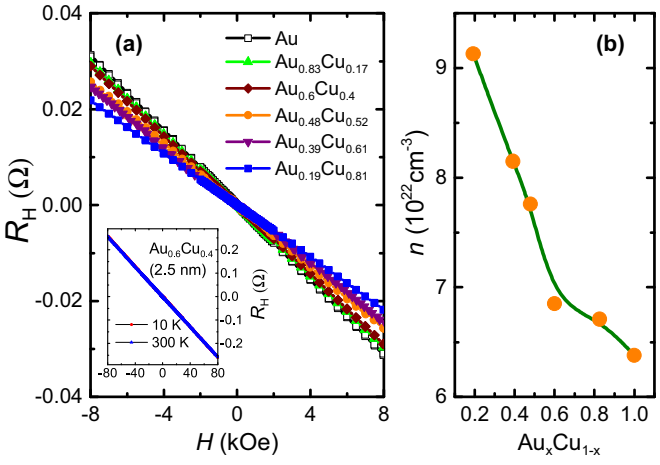

FIG. 2. (a) Hall effect curves of YIG/Au-Cu(2.5 nm) with different Au concentrations at room temperature. Inset shows Hall curves of YIG/$Au_{0.6}Cu_{0.4}$(2.5 nm) at 10 K (red circle) and 300 K (blue triangle). (b) Au atomic fraction dependence of carrier concentration.

spin Hall AHE, in striking contrast to YIG/Pt, Pd, Ta, and W systems. It should be stressed that spin Hall AHE was derived to be proportional to the square of the spin Hall angle [27]. Considering that the Au-Cu samples in comparison with pure Au exhibit larger SSE with a much larger spin Hall angle at the near equiatomic composition, which is comparable to that of Pt and will be given later, there is little possibility that the Au-Cu samples (including pure Au) coincidently have finite but canceled spin Hall AHE and normal AHE induced by MPE. Therefore, the YIG/Au-Cu system is an ideal large SHE model structure free from MPE with negligible imaginary spin mixing conductance.

Parenthetically, from the Hall slope of the YIG/Au-Cu samples, the charge carrier density (n) of Au-Cu alloys is determined and shown in Fig. 2(b). The value of n for pure Au is about 6.4×10^{22} cm^{-3}, consistent with the gold bulk value of 5.9×10^{22} cm^{-3} [29]. With decreasing Au concentration, n monotonically increases to 9.1×10^{22} cm^{-3} for $Au_{0.19}Cu_{0.81}$. In addition, the R_H-H loops at low and room temperatures are overlapped with each other, as indicated in the inset of Fig. 2(a). It means that the carrier density of Au-Cu alloys in the hybrid structure is insensitive to temperature, in striking contrast to great changes in charge carrier density or even the charge carrier type for the YIG/Pt structure [13].

C. Spin diffusion length

Besides spin Hall AHE, theoretical spin Hall magnetoresistance (SMR) was also derived from the real part of the interface spin mixing conductance in the hybrid structure [27,30]. Although there is absence of spin Hall AHE in the YIG/Au-Cu structure, we do identify appreciable SMR and further quantify the spin Hall angle of the near equiatomic Au-Cu alloy by systematically characterizing the SMR results after the evaluation of the spin diffusion length from the SSE (or ISHE) results.

As is known, in the thermally induced spin current injection model with LSSE setup [14], the measured ISHE voltage can be expressed as a function of metal layer thickness t as Eq. (1):

$$\Delta V_{th}(t) = 2[CL\nabla T][\rho(t)\theta_{SH}][(\lambda_{SF}/t)\tanh(t/2\lambda_{SF})], \quad (1)$$

where C is the spin current injection coefficient involving spin mixing conductance, L is the length of the Hall bar long axis, ∇T is the temperature gradient, and ρ is the film resistivity. The ISHE voltage and film resistivity were measured for the series $Au_{0.6}Cu_{0.4}$ films with thickness ranging from 6 to 60 nm deposited on the YIG cut from the same specimen. Figure 3 shows the thickness dependence of ISHE voltage divided by the film resistivity. One can note a pretty good fitting of the experiment data by using Eq. (1), which gives a spin diffusion length of 4.6 nm for $Au_{0.6}Cu_{0.4}$.

For comparison, the series YIG/Au control samples were also characterized and the corresponding data are shown in the inset of Fig. 3. The similar data fitting gives a spin diffusion length of about 9.4 nm for Au. The value of Au-Cu is only about half of this number. The Au spin diffusion length might be underestimated here, judging from the relatively poor fitting at the thick Au region. For a reliable fitting, more data from the thicker samples are needed for such a large spin diffusion length, but the corresponding ISHE voltage is too small to

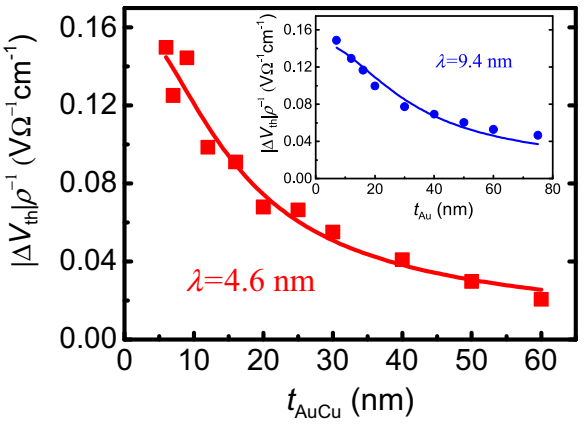

FIG. 3. Thickness dependence of thermal voltage divided by resistivity of $Au_{0.6}Cu_{0.4}$ and Au. Red square corresponds to experimental data and red line denotes fitting result with Eq. (1).

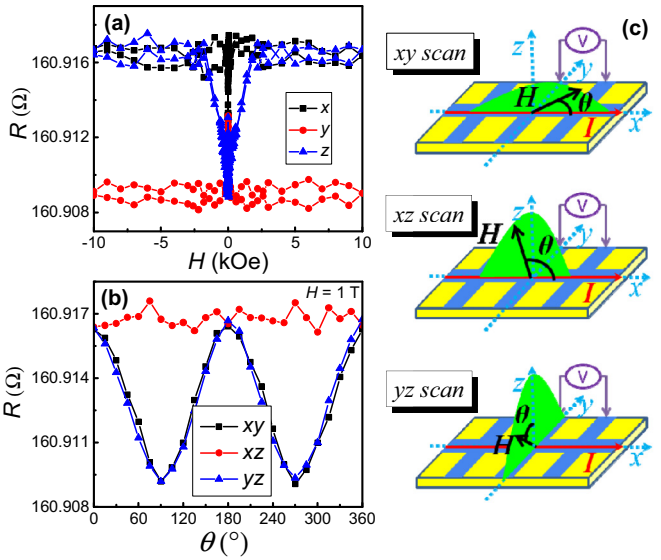

FIG. 4. (a) Magnetic field dependence of magnetoresistance in YIG/$Au_{0.6}Cu_{0.4}$(5.5 nm) when H was applied in x (black square), y (red circle), and z (blue triangle) direction. (b) Angular dependence of magnetoresistance in YIG/$Au_{0.6}Cu_{0.4}$(5.5 nm) at 1-T magnetic field when H is rotated in the xy (black square), xz (red circle), and yz (blue triangle) plane, respectively, as illustrated in (c).

be measured for the Au samples. We would like to point out that the spin diffusion length depends on the film thickness or strictly the film resistivity as demonstrated by Niimi *et al.* [31]. A rapid increase of the resistivity occurs at the metal layer thickness below 15 nm for both $Au_{0.6}Cu_{0.4}$ and Au samples, which could be ascribed to the increased surface/interface scattering. When the thickness is beyond 15 nm, however, the resistivity changes little. Therefore, it is reasonable to assume a constant spin diffusion length for the $Au_{0.6}Cu_{0.4}$ alloy films, considering that most samples have a thickness exceeding 15 nm in data fitting. For the Au samples with a much larger spin diffusion length, the lack of data points at the thicker Au region may lead to an underestimated spin diffusion length because the thin Au samples with enhanced resistivity and thus reduced spin diffusion length may be weighted too much. Based on these results, it is undoubted that the spin diffusion length of Au is significantly shortened after alloying with Cu. This should be correlated with the intensive atomic disorder scattering. Empirically the transition metals with a large spin Hall angle usually have a short spin diffusion length [14]. However, the thermal spin current injection model alone cannot further give the absolute value of spin Hall angle from the ISHE results.

D. Magnetoresistance measurements and spin Hall angle

In the theory of SMR, the spin current generated in a nonmagnetic metal (NM) layer due to SHE will be reflected (or absorbed) at the YIG/NM interface when the polarization vector of the spin current is parallel (or perpendicular) to the YIG magnetization M. The former gives rise to a low-resistance state due to the ISHE of the reflected spin current, whereas the latter leads to a high-resistance state with little spin current reflection because of the spin transfer torque (STT) [27]. The SMR has a well-defined angular dependent expression as

$$R \approx R_0 + \Delta R\left(1 - m_y^2\right), \tag{2}$$

where m_y stands for the y component of unit magnetization vector of YIG, and ΔR is always a positive value, depending on the spin Hall angle, the spin diffusion length, and the structure and interface parameters. In the limit where the spin current transverse to m is completely absorbed as an STT without reflection, maximum magnetoresistance (MR) has the form of

$$\left(\frac{\Delta R}{R_0}\right)_{\mathrm{SMR}} \approx \theta_{\mathrm{SH}}^2 \frac{\lambda}{d_N} \tanh\frac{d_N}{\lambda} \tanh^2\frac{d_N}{2\lambda}, \tag{3}$$

where θ_{SH}, λ, d_N denote spin Hall angle, spin diffusion length, and thickness of nonmagnetic metal film, respectively. It was reported that this ideal situation is not so far from reality in YIG/noble metals [32,33].

We systematically measured the MR of the YIG/Au-Cu samples. Figure 4(a) gives an example of field dependence of resistance in YIG/$Au_{0.6}Cu_{0.4}$ (5.5 nm) with H applied in the x, y, and z axes. Clearly it exhibits an anisotropic magnetoresistance (AMR) -like attribute as tuned by the magnetization direction of YIG. The MR ratio is about 5×10^{-5}, much smaller than the conventional AMR value (10^{-2}). Figure 4(b) shows the corresponding angular dependence of MR with a constant 1-T field rotating in the xy, yz, and xz plane. A perfect $\cos^2\theta$ relation is observed for the xy and yz results, and they coincide with each other. When H is rotated in the xz plane, namely, m_y remains zero, the sample resistance almost stays constant. These MR features exactly follow what the SMR theory describes in Eq. (2). Therefore, the MR observed in YIG/Au-Cu samples should completely come from SMR considering that the present sample is free from MPE.

The MR ratios of all YIG/$Au_{0.6}Cu_{0.4}$ samples are summarized in Fig. 5. On the whole, the SMR gradually decreases as the Au-Cu thickness increases. Some scattered data points may be caused by the tiny quality difference from sample to sample, although the series films were deposited on the YIG cut from the same specimen in a single sputtering run. Using Eq. (3), the

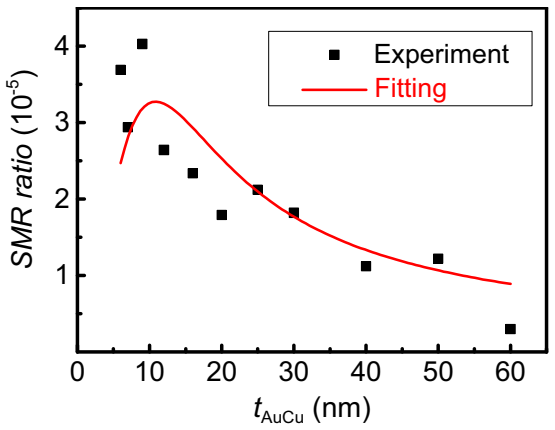

FIG. 5. Thickness dependence of SMR ratio in $Au_{0.6}Cu_{0.4}$. Black square corresponds to experimental data and red line denotes fitting with Eq. (3).

SMR data of the YIG/$Au_{0.6}Cu_{0.4}$ samples can be fitted with the fitting curve also plotted in Fig. 5. The theoretical result does not nicely match most of the experimental data points, but still looks reasonable. It renders a spin Hall angle of about 0.011 for $Au_{0.6}Cu_{0.4}$, almost equal to the first-principle calculation result [23]. The large spin Hall angle of $Au_{0.6}Cu_{0.4}$ is comparable with that of Pt without considering the controversial MPE [14]. We would like to point out that the SMR in the YIG/Au control samples is also identified when the Au layer is thinner than 30 nm, but the magnitude of SMR is about two to five times smaller than those of the YIG/$Au_{0.6}Cu_{0.4}$ samples. For thicker Au samples, the SMR signal is below the noise level of the measurement system with accurancy of $\Delta R/R = 2 \times 10^{-6}$. Therefore, the spin Hall angle of Au cannot be safely obtained from the very limited SMR data. In comparison with the Au spin Hall angle reported previously [14], the Au-Cu spin Hall angle is enhanced at least two to three times caused by the extrinsic mechanism.

IV. CONCLUSION

In summary, we systematically investigated the spin Seebeck effect, spin Hall AHE, and spin Hall magnetoresistance in the YIG/Au-Cu hybrid structure. Our results suggest that apart from the case of diluted alloys, atomic disorder scattering in the concentrated alloys can give rise to large enhancement of spin Hall effect. The absence of AHE and spin Hall AHE in the Au-Cu hybrid structure suggests the nonexistence of MPE. Based on a thermally induced spin current model and spin Hall magnetoresistance theory, we determined the spin diffusion length and spin Hall angle of $Au_{0.6}Cu_{0.4}$ to be about 4.6 nm and 0.011, respectively. The present results demonstrate that Au-Cu alloy is an ideal material for pure spin current study and spintronic application.

ACKNOWLEDGMENTS

This work was supported by the National Basic Research Program of China under Grant No. 2015CB921403, and the National Natural Science Foundation of China under Grants No. 51371191 and No. 51431009.

[1] L. Vila, T. Kimura, and Y. Otani, Phys. Rev. Lett. **99**, 226604 (2007).
[2] J. E. Hirsch, Phys. Rev. Lett. **83**, 1834 (1999).
[3] T. Jungwirth, J. Wunderlich, and K. Olejnik, Nat. Mater. **11**, 382 (2012).
[4] Y. Tserkovnyak, A. Brataas, and G. E. W. Bauer, Phys. Rev. Lett. **88**, 117601 (2002).
[5] E. Saitoh, M. Ueda, H. Miyajima, and G. Tatara, Appl. Phys. Lett. **88**, 182509 (2006).
[6] Y. Kajiwara, K. Harii, S. Takahashi, J. Ohe, K. Uchida, M. Mizuguchi, H. Umezawa, H. Kawai, K. Ando, K. Takanashi, S. Maekawa, and E. Saitoh, Nature **464**, 262 (2010).
[7] K. Uchida, S. Takahashi, K. Harii, J. Ieda, W. Koshibae, K. Ando, S. Maekawa, and E. Saitoh, Nature **455**, 778 (2008).
[8] R. Karplus and J. M. Luttinger, Phys. Rev. **95**, 1154 (1954).
[9] M. I. Dyakonov and V. I. Perel, Phys. Lett. A **35**, 459 (1971).
[10] Y. K. Kato, R. C. Myers, A. C. Gossard, and D. D. Awschalom, Science **306**, 1910 (2004).
[11] K. Uchida, M. Ishida, T. Kikkawa, A. Kirihara, T. Murakami, and E. Saitoh, J. Phys.: Condens. Matter **26**, 343202 (2014).
[12] S. Y. Huang, X. Fan, D. Qu, Y. P. Chen, W. G. Wang, J. Wu, T. Y. Chen, J. Q. Xiao, and C. L. Chien, Phys. Rev. Lett. **109**, 107204 (2012).
[13] Y. M. Lu, Y. Choi, C. M. Ortega, X. M. Cheng, J. W. Cai, S. Y. Huang, L. Sun, and C. L. Chien, Phys. Rev. Lett. **110**, 147207 (2013).
[14] D. Qu, S. Y. Huang, B. F. Miao, S. X. Huang, and C. L. Chien, Phys. Rev. B **89**, 140407(R) (2014).
[15] H. Ibach and H. Luth, *Solid-State Physics: An Introduction to Principles of Materials Science* (Springer, Berlin, 2009).
[16] D. A. Papaconstantopoulos, *Handbook of Band Structure of Elemental Solids* (Plenum, New York, 1986).
[17] Y. Niimi, Y. Kawanishi, D. H. Wei, C. Deranlot, H. X. Yang, M. Chshiev, T. Valet, A. Fert, and Y. Otani, Phys. Rev. Lett. **109**, 156602 (2012).
[18] Y. Niimi, M. Morota, D. H. Wei, C. Deranlot, M. Basletic, A. Hamzic, A. Fert, and Y. Otani, Phys. Rev. Lett. **106**, 126601 (2011).
[19] A. Fert and P. M. Levy, Phys. Rev. Lett. **106**, 157208 (2011).
[20] Y. Niimi, H. Suzuki, Y. Kawanishi, Y. Omori, T. Valet, A. Fert, and Y. Otani, Phys. Rev. B **89**, 054401 (2014).
[21] P. Laczkowski, J. C. Rojas-Sánchez, W. Savero-Torres, H. Jaffrès, N. Reyren, C. Deranlot, L. Notin, C. Beigné, A. Marty, J. P. Attané, L. Vila, J. M. George, and A. Fert, Appl. Phys. Lett. **104**, 142403 (2014).
[22] M. Gradhand, D. V. Fedorov, P. Zahn, and I. Mertig, Phys. Rev. B **81**, 245109 (2010).
[23] S. Wimmer, D. Ködderitzsch, K. Chadova, and H. Ebert, Phys. Rev. B **88**, 201108(R) (2013).
[24] T. Kikkawa, K. Uchida, Y. Shiomi, Z. Qiu, D. Hou, D. Tian, H. Nakayama, X. F. Jin, and E. Saitoh, Phys. Rev. Lett. **110**, 067207 (2013).
[25] Y. Zhu and J. W. Cai, Appl. Phys. Lett. **87**, 032504 (2005).

[26] Y. M. Lu, J. W. Cai, H. Y. Pan, and L. Sun, Appl. Phys. Lett. **100**, 022404 (2012).
[27] Y. T. Chen, S. Takahashi, H. Nakayama, M. Althammer, S. T. B. Goennenwein, E. Saitoh, and G. E. W. Bauer, Phys. Rev. B **87**, 144411 (2013).
[28] D. Qu, S. Y. Huang, J. Hu, R. Q. Wu, and C. L. Chien, Phys. Rev. Lett. **110**, 067206 (2013).
[29] C. L. Chien and C. R. Westgate, *The Hall Effect and Its Applications* (Plenum, New York, 1980).
[30] M. Althammer, S. Meyer, H. Nakayama, M. Schreier, S. Altmannshofer, M. Weiler, H. Huebl, S. Geprägs, M. Opel, R. Gross, D. Meier, C. Klewe, T. Kuschel, J. M. Schmalhorst, G. Reiss, L. M. Shen, A. Gupta, Y. T. Chen, G. E. W. Bauer, E. Saitoh *et al.*, Phys. Rev. B **87**, 224401 (2013).
[31] Y. Niimi, D. Wei, H. Idzuchi, T. Wakamura, T. Kato, and Y. Otani, Phys. Rev. Lett. **110**, 016805 (2013).
[32] X. Jia, K. Liu, K. Xia, and G. E. W. Bauer, Europhys. Lett. **96**, 17005 (2011).
[33] C. Burrowes, B. Heinrich, B. Kardasz, E. A. Montoya, E. Girt, Y. Y. Sun, Y. Y. Song, and M. Z. Wu, Appl. Phys. Lett. **100**, 092403 (2012).